THE JOURNAL OF BIOLOGICAL CHEMISTRY VOL. 286, NO. 20, pp. 18213–18221, May 20, 2011
Printed in the U.S.A.

Ligand Binding Induces an Ammonia Channel in 2-Amino-2-desoxyisochorismate (ADIC) Synthase PhzE*[S]

Received for publication, September 9, 2010, and in revised form, February 28, 2011 Published, JBC Papers in Press, March 29, 2011, DOI 10.1074/jbc.M110.183418

Qi-Ang Li[‡1], Dmitri V. Mavrodi[§], Linda S. Thomashow[§¶], Manfred Roessle[‖], and Wulf Blankenfeldt[‡2]

From the [‡]Department of Physical Biochemistry, Max Planck Institute of Molecular Physiology, Otto-Hahn-Strasse 11, 44227 Dortmund, Germany, the [§]Department of Plant Pathology, Washington State University, Pullman, Washington 99164-6430, the [¶]Agricultural Research Service, Root Disease and Biological Control Unit, United States Department of Agriculture, Pullman, Washington 99164-6430, and the [‖]European Molecular Biology Laboratory-Hamburg Outstation, c/o Deutsches Elektronen-Synchrotron, 22603 Hamburg, Germany

PhzE utilizes chorismate and glutamine to synthesize 2-amino-2-desoxyisochorismate (ADIC) in the first step of phenazine biosynthesis. The PhzE monomer contains both a chorismate-converting menaquinone, siderophore, tryptophan biosynthesis (MST) and a type 1 glutamine amidotransferase (GATase1) domain connected by a 45-residue linker. We present here the crystal structure of PhzE from *Burkholderia lata* 383 in a ligand-free open and ligand-bound closed conformation at 2.9 and 2.1 Å resolution, respectively. PhzE arranges in an intertwined dimer such that the GATase1 domain of one chain provides NH_3 to the MST domain of the other. This quaternary structure was confirmed by small angle x-ray scattering. Binding of chorismic acid, which was found converted to benzoate and pyruvate in the MST active centers of the closed form, leads to structural rearrangements that establish an ammonia transport channel approximately 25 Å in length within each of the two MST/GATase1 functional units of the dimer. The assignment of PhzE as an ADIC synthase was confirmed by mass spectrometric analysis of the product, which was also visualized at 1.9 Å resolution by trapping in crystals of an inactive mutant of PhzD, an isochorismatase that catalyzes the subsequent step in phenazine biosynthesis. Unlike in some of the related anthranilate synthases, no allosteric inhibition was observed in PhzE. This can be attributed to a tryptophan residue of the protein blocking the potential regulatory site. Additional electron density in the GATase1 active center was identified as zinc, and it was demonstrated that Zn^{2+}, Mn^{2+}, and Ni^{2+} reduce the activity of PhzE.

Chorismic acid is the precursor for a large number of primary and secondary metabolites such as *e.g.* the aromatic amino acids, ubiquinone, folate, vitamin K, and the siderophores enterobactin and pyochelin. Because the production and utilization of chorismic acid are limited to prokaryotic microorganisms and plants, enzymes involved in chorismate metabolism are attractive targets for the development of biologically active compounds as exemplified by the herbicide glyphosate, which inhibits an enzyme of the shikimate pathway required for chorismate biosynthesis.

Four chorismate-utilizing enzyme families are known (1). First, two unrelated types of chorismate mutases, AroH and AroQ, generate prephenate as a precursor of phenylalanine and tyrosine. A third family consists of the chorismate lyases, which cleave chorismic acid to *p*-hydroxybenzoate and pyruvate in the biosynthesis of ubiquinone. Finally, the fourth group comprises members of the menaquinone, siderophore, tryptophan (MST)[3] biosynthesis family, which utilize water or ammonia to perform nucleophilic substitution at the six-membered ring of chorismate with or without concomitant rearrangement of the double bond system in an Mg^{2+}-dependent reaction (Fig. 1). Of these enzymes, isochorismate, 2-amino-2-desoxyisochorismate (ADIC), and 4-amino-4-desoxychorismate synthases release the isomerized product, whereas anthranilate (AS) and salicylate synthase initiate a subsequent sigmatropic elimination of pyruvate within the same active center, leading to the synthesis of anthranilate or salicylate, respectively (2, 3). The aminating members of the MST family generate ammonia from glutamine in a type 1 glutamine amidotransferase (GATase1) domain, which either forms a heterodimer with or is fused to the N or C terminus of the MST domain. It is believed that glutamine hydrolysis by GATase1 is only initiated once chorismate has bound to the MST domain and that NH_3 is delivered through a tunnel to the chorismate binding site to avoid its loss to the solvent (4, 5).

Crystallographic and biochemical studies have led to considerable structural and mechanistic insight into members of the MST family in recent years, yet structures of a MST/GATase1 fusion protein and of an ADIC synthase are lacking. In addition, the existence of an intramolecular channel has never been demonstrated in these enzymes. We have aimed at filling these gaps

* This work was supported by Deutsche Forschungsgemeinschaft Grant BL587/1-1/2 (to W. B.).

[S] The on-line version of this article (available at http://www.jbc.org) contains Experimental Procedures and additional references, Figs. S1–S9, and Tables S1 and S2.

The atomic coordinates and structure factors (codes 3R74, 3R75, 3R76, and 3R77) have been deposited in the Protein Data Bank, Research Collaboratory for Structural Bioinformatics, Rutgers University, New Brunswick, NJ (http://www.rcsb.org/).

[1] Supported by the International Max Planck Research School in Chemical Biology.

[2] To whom correspondence should be addressed: Lehrstuhl für Biochemie, Universität Bayreuth, Universitätsstrasse 30, 95447 Bayreuth, Germany. Tel.: 49-921-552427; Fax: 49-921-552432; E-mail: wulf.blankenfeldt@uni-bayreuth.de.

[3] The abbreviations used are: MST, menaquinone, siderophore, tryptophan; ADIC, 2-amino-2-desoxyisochorismate; AS, anthranilate synthase; BisTris propane, 2-[bis(2-hydroxyethyl)amino]-2-(hydroxymethyl)propane-1,3-diol; GATase1, glutamine amidotransferase type 1; PDB, Protein Data Bank; SAXS, small angle x-ray scattering.

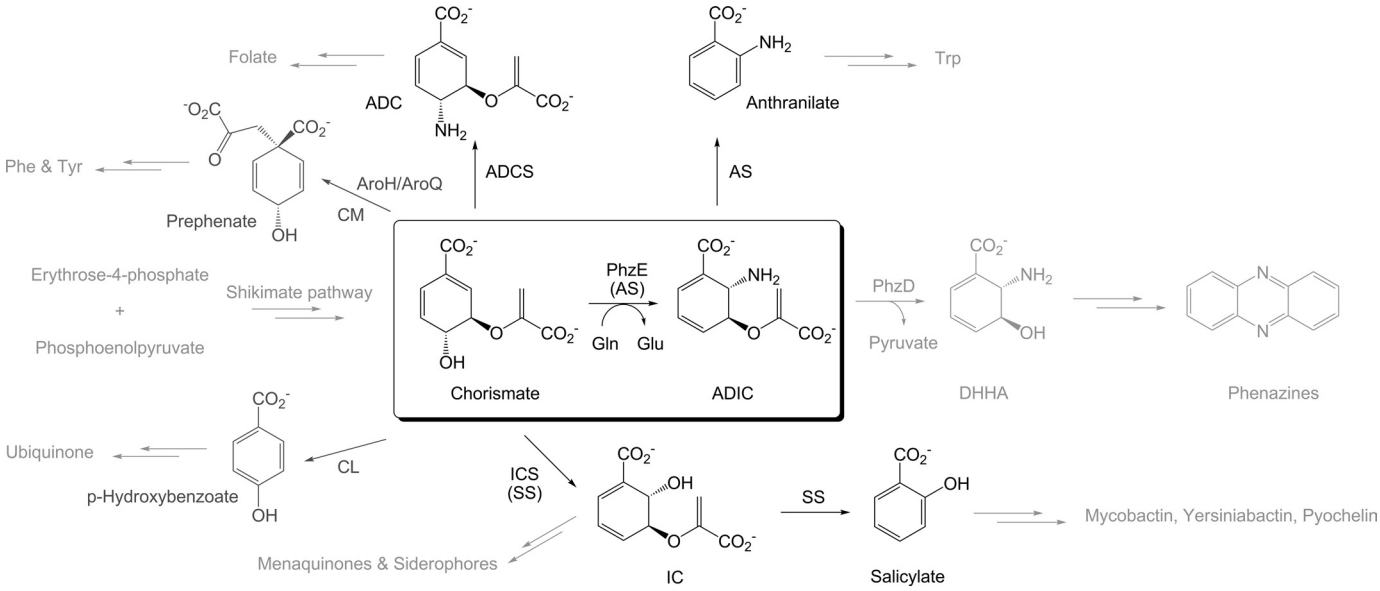

FIGURE 1. **Biochemical conversions of chorismate.** Reactions not directly involved in chorismate turnover are shown in *light gray*, and chorismate conversions not involving members of the MST family are shown in *dark gray*. *CM*, chorismate mutases of the AroH and AroQ type; *CL*, chorismate lyase, *ADCS*, 4-amino-4-desoxychorismate synthase; *ICS*, isochorismate synthase; *SS*, salicylate synthase; DHHA, *trans*-2,3-dihydro-3-hydroxoanthranilate.

by determining the crystal structure of ADIC synthase PhzE from *Burkholderia lata* 383, an enzyme that consists of an MST/GATase1 fusion in a single chain, in an uncomplexed open and a ligand-bound closed conformation. In addition, we have measured small angle x-ray scattering (SAXS) and biochemical data. PhzE catalyzes the first step in the biosynthesis of phenazines, a class of redox-active secondary metabolites that a number of bacterial strains produce as virulence factors, antibiotics, and probably also as respiratory pigments (6, 7). Because PhzE commits chorismate to phenazine biosynthesis, we also investigated whether the enzyme is subject to feedback inhibition similar to some of the related anthranilate synthases. In addition, we confirmed the functional assignment of PhzE as an ADIC synthase by mass spectrometry and by visualizing PhzE-produced ADIC in the active center of an inactive mutant of PhzD from *Pseudomonas fluorescens* 2-79. PhzD is an isochorismatase that catalyzes the step following PhzE in phenazine biosynthesis. Together, our new data extend the spectrum of structurally characterized MST proteins to ADIC synthases and also provide new insights into several mechanistic aspects of this enzyme family.

EXPERIMENTAL PROCEDURES

For full experimental details, refer to the supplemental material.

Overexpression and Purification of B. lata 383 PhzE and of P. fluorescens 2-79 PhzD—B. lata phzE was amplified from genomic DNA and cloned into a modified pET vector extending the protein for an N-terminal protease-cleavable His_6 tag. After overexpression in *Escherichia coli* and purification on immobilized Ni^{2+}, the tag was cleaved with tobacco etch virus protease, and the protein was further purified by size exclusion chromatography. Preparation of PhzD from *P. fluorescens* 2-79 was achieved with a similar protocol. Seleno-L-methionine labeling of PhzE was performed by the methionine biosynthesis suppression method (8), and mutations were introduced into PhzE and PhzD with the QuikChange method (Stratagene).

Crystallization, Data Collection, and Structure Determination—Crystals of ligand-free *B. lata* PhzE (native and seleno-L-methionine-labeled) were obtained at room temperature by the hanging-drop vapor diffusion method with a 500-μl reservoir consisting of 0.1 M BisTris propane, pH 7.0, 0.2 M KSCN, and 22% (w/v) PEG 3350, of which 1 μl was mixed with 2 μl of protein solution containing 1 mM $MgCl_2$ and 20 mM glutamine. For the ligand-bound form, the protein was incubated with 50 mM $MgCl_2$, 20 mM chorismate, and 25 mM L-glutamine for 30 min before crystallization against a reservoir containing 0.1 M HEPES buffer, pH 7.1, 0.2 M $MgCl_2$, and 15% isopropyl alcohol at 4 °C. Streak seeding was required to obtain suitable crystals. To remove Zn^{2+} bound to the GATase1 active site in the complex structure (see below), PhzE was incubated with 10 mM EDTA followed by buffer exchange prior to setting up crystallization experiments.

Crystals of the D38A mutant of PhzD from *P. fluorescens* 2-79 were obtained with a precipitant consisting of 0.1 M sodium cacodylate, pH 6.5, 0.2 M sodium acetate, and 25% (w/v) PEG 4000. They were soaked for 1 h in a solution containing 0.1 M BisTris, pH 6.5, 20% (w/v) PEG 4000, 0.1 M NaCl, and 1 mM ADIC. ADIC was synthesized enzymatically and purified by HPLC as described in the supplemental materials.

Diffraction data of cryoprotected PhzE crystals were collected on a MX-225 CCD detector (marresearch) at beamline X10SA of the Swiss Light Source (Paul Scherrer Institute, Villigen, Switzerland) and integrated with XDS (9). The structure of apo-PhzE was determined from selenium MAD data, using SHELXD (10) and SHARP (11) for initial phasing. The model was traced in O (12) and refined with REFMAC5 (13). Final corrections were applied in COOT (14). The refined structure was used for molecular replacement of the ligand-bound form in PHASER (15). Ligand restraints dictionaries were generated

TABLE 1
Data collection and refinement statistics.

Parameters	Open PhzE	Closed PhzE + Zn^{2+}	Closed PhzE	PhzD-D38A/ADIC
Data collection				
Space group	$P6_222$	$P2_12_12$	$P2_12_12$	$P2_12_12_1$
Cell dimensions				
a, *b*, *c* (Å)	172.4, 172.4, 216.4	259.7, 94.5, 53.6	258.2, 97.8, 54.0	68.5, 72.1, 79.0
α, β, γ (°)	90, 90, 120	90, 90, 90	90, 90, 90	90, 90, 90
Resolution (Å)[2]	20-2.9 (3.0-2.9)	20-2.1 (2.2-2.1)	20-2.6 (2.7-2.6)	50-1.9 (2.0-1.9)
R_{sym} (I)	7.0 (52.5)	6.6 (30.5)	6.9 (41.2)	5.0 (28.0)
I/σ (I)	20.1 (3.7)	12.4 (3.7)	17.7 (4.5)	18.7 (4.9)
Completeness (%)	99.6 (99.9)	98.3 (98.3)	99.8 (100)	97.7 (98.2)
Redundancy	4.8 (4.9)	2.2 (2.2)	4.0 (4.1)	2.5 (2.4)
Refinement				
Resolution (Å)[2]	20-2.9 (3.0-2.9)	20-2.1 (2.15-2.1)	20-2.6 (2.65-2.6)	20-1.9 (1.95-1.9)
No. reflections	204850 (42476)	324405 (146170)	173817 (43071)	29748 (2271)
R_{work}	18.7 (25.5)	14.6 (17.4)	16.8 (22.0)	14.3 (25.2)
R_{free}	23.1 (32.4)	20.0 (22.4)	23.5 (34.3)	19.2 (33.1)
No. atoms/*B*-factors (Å[2])				
Protein	9088/31	10439/30	9119/30	3239/23
Ligand/ion	-/-	45/33	42/34	36/24
Water	80/56	812/53	332/28	454/33
Root mean square deviations				
Bond lengths/angles (Å/°)	0.017/1.693	0.023/1.901	0.016/1.576	0.025/1.904
PDB entry code	3R74	3R75	3R76	3R77

with PRODRG (16). Diffraction data of cryoprotected *P. fluorescens* 2-79 PhzD crystals were collected at 100 K on a mar345 image plate (marresearch) using a Micro-MAX-007 HF rotating copper anode (Rigaku) as x-ray source. The structure was solved by molecular replacement using coordinates of *Pseudomonas aeruginosa* PhzD (Protein Data Bank (PDB) ID code 1NF8) (17). Full data collection and refinement statistics are shown in Table 1 and supplemental Table S2.

SAXS—SAXS experiments were performed at beamline X33 of the DORIS III storage ring (DESY and EMBL Hamburg, Germany) (18), using concentrations of 3 and 6 mg/ml PhzE to assess protein interactions. Bovine serum albumin (BSA) was taken as a reference for calculating the molecular mass of PhzE particles in solution. Data were processed with PRIMUS (19), using GNOM (20) to compute forward scattering, radius of gyration and distance distribution.

Low resolution models of PhzE were built with DAMMIN (21), applying a 2-fold symmetry constraint. Finally, 10 independent reconstructions were superimposed with SUBCOMP and DAMAVER (21) to derive the most probable PhzE model after filtering to the molecular mass of the dimer.

Isothermal Titration Calorimetry—Isothermal titration calorimetry measurements were performed at 25 °C with a VP-ITC system from MicroCal LLC. PhzE was diluted to 100 μM in buffer containing 50 mM Tris, pH 7.5, and 150 mM NaCl with or without 1 mM $MgCl_2$. Chorismate was dissolved in the same buffer as used for the protein to a final concentration of 1 mM. Data were analyzed with Origin version 7 (OriginLab Corporation).

Enzymatic Activity Assays—Activity assays were performed by modification of a previously described method (22). Reaction mixtures contained 0.1 M HEPES-Na, pH 7.0, 1 mM $MgCl_2$, 20 mM glutamine, and 1–50 μM chorismic acid at 25 °C. The reaction was initiated by addition of PhzE to a final concentration of 100 nM, and initial velocities were determined by following the increase in absorption at 280 nm. K_m, and k_{cat} values were determined by fitting to a Michaelis-Menten equation in GraFit (Erithacus Software). Experiments were repeated at least in triplicate. Turnover of ADIC by PhzD was confirmed by HPLC.

RESULTS

PhzE Is an ADIC Synthase—ADIC is an intermediate of anthranilate biosynthesis (23), but rather than being released from the PhzE-related AS, it is further converted to anthranilate within the active site of the MST domain of this enzyme. ADIC was first postulated as a phenazine precursor in 1982 (24), and full incorporation of ADIC into phenazines has been demonstrated (25), but direct proof of its generation and release from PhzE has not been brought forward. In fact, the role of PhzE as an ADIC synthase has recently been questioned due to the finding that PhzE could complement an AS mutant of *E. coli* (26) and because it possesses only 12% sequence identity to and a different domain arrangement than SgcD, an ADIC synthase involved in the biosynthesis of the enediyne antitumor antibiotic C-1027 (27).

We therefore investigated the product of PhzE by several methods, which are detailed in the supplemental materials. First, incubation of chorismic acid with glutamine, $MgCl_2$, and PhzE produced a species with increased absorption at 280 nm (supplemental Fig. S1*A*), as has been described for ADIC previously (22). The compound possessed the expected molecular mass (supplemental Fig. S1*B*) and could further be converted to *trans*-2,3-dihydro-3-hydroxyanthranilic acid with PhzD (supplemental Fig. S1*C*), an isochorismatase that catalyzes the step following PhzE in phenazine biosynthesis (17). In addition, it was possible to visualize ADIC at 1.9 Å resolution in crystals of the inactive D38A mutant of PhzD from *P. fluorescens* 2-79 by soaking with HPLC-purified product of PhzE (R_{work} = 16.4%, R_{free} = 21.0%; supplemental Fig. S1*D*). Together, this confirms the assignment of PhzE as an ADIC synthase.

After treatment with EDTA to remove bound Zn^{2+} (see below), enzyme parameters for chorismic acid were $K_m = 2.4 \pm 0.5$ μM and $k_{cat} = 0.3 \pm 0.01$ s^{-1} for chorismic acid, which is similar to other MST enzymes (supplemental Table S1). Unlike

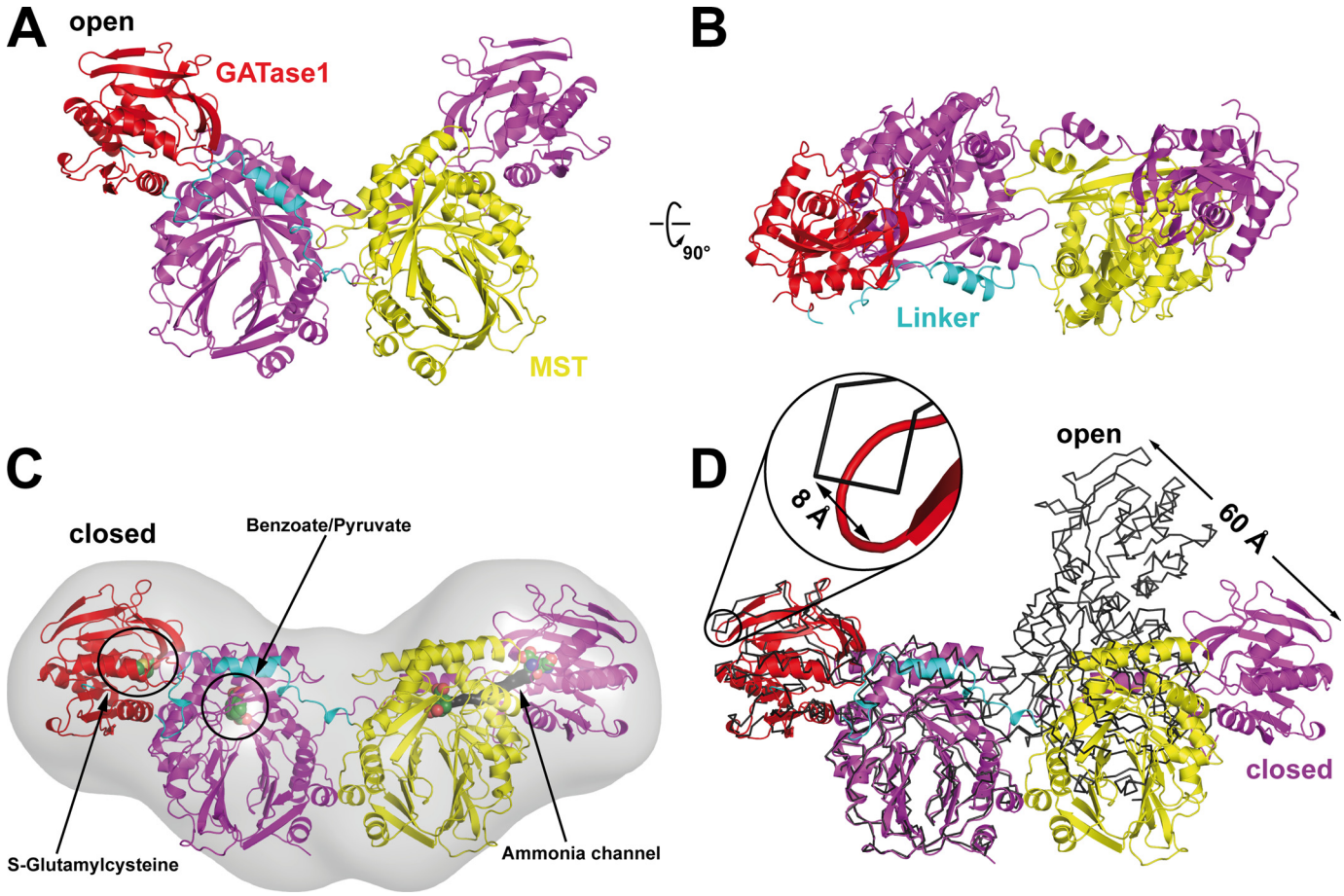

FIGURE 2. **Overall structure of PhzE.** *A*, ligand-free open form. One chain has been colored in *magenta*, the other monomer is colored according to domains. *B*, same as in *A*, but seen from the *top*. *C*, ligand-bound closed form, fitted to the SAXS envelope (*gray*) with SITUS (37). *Circles* indicate the positions of active sites in the MST and GATase1 domain. Ligands are shown in *ball-and-stick* representation. The NH_3 channel (*black mesh*) was located with CAVER (30). *D*, comparison of the open (*thin lines*) and closed structure (*ribbons*) by superimposition of one MST domain from each crystal form. Note that although the interaction within the functional MST/GATase1 units does not change considerably, distortion of the MST/MST interface leads to a large apparent movements within the dimer. This figure was prepared with PyMOL.

some AS, PhzE was not inhibited by tryptophan or by phenazine biosynthesis intermediates.

Crystallization and Structure Determination of PhzE—It was not possible to obtain crystals with PhzE from several *Pseudomonas* spp., which we initially investigated because pseudomonads are the best studied phenazine producers. Crystallization experiments were therefore extended to the protein of *B. lata* 383, which possesses the same domain arrangement as the *Pseudomonas* orthologs at an average sequence identity of 56% (supplemental Fig. S2). Crystals of ligand-free *B. lata* 383 PhzE diffracted to 2.9 Å, and the structure was determined by anomalous diffraction data from crystals of seleno-L-methionine-labeled protein. The model was refined to R_{work} = 18.7% (R_{free} = 23.1%) and could, with exception of the termini and two flexible regions, be traced completely (missing residues in chain A: Met^{1}–Pro^{5}, Gly^{429}–Leu^{439}, Arg^{634}–Ala^{643}; chain B: Met^{1}–Asn^{6}, Thr^{28}–Glu^{33}, Glu^{433}–Leu^{439}, Lys^{637}–Ala^{643}).

The structure of PhzE crystallized in the presence of glutamine, chorismic acid and Mg^{2+} was solved by molecular replacement. These crystals diffracted to 2.1 Å, and the refinement converged at R_{work} = 14.4% and R_{free} = 20.0%, and the final model showed a similar amount of disorder as the apo structure. Data collection and refinement statistics are shown in Table 1 and supplemental Table S2.

Overall Structure of PhzE—Size exclusion chromatography indicated that PhzE forms homodimers in solution, and indeed one 140-kDa homodimer was found in the asymmetric unit of both crystal forms investigated here. We initially determined the structure of PhzE crystallized in the absence of ligands, which will be referred to as the open form. In this crystal form, the dimer adopts a butterfly-shaped structure in which the N-terminal chorismate-binding MST domains (residues 1–395) lie near the 2-fold symmetry axis of the dimer and the GATase1 domains (residues 442–643) occupy the far ends of the wings (Fig. 2*A*). The linker (residues 396–441) is partially disordered (Gly^{429}–Leu^{439} and Glu^{433}–Leu^{439} missing in chain A and chain B, respectively), but crystal packing and tracing considerations only allow for an intertwined dimer in which the GATase1 of chain A is in intimate contact with the MST domain of chain B and vice versa. This indicates that the functional unit is established by the MST domain of one chain and the GATase1 of the other. The quaternary structure of PhzE is unprecedented within the MST family, and to exclude that the dimer is a crystallization artifact, we performed SAXS experiments that confirmed

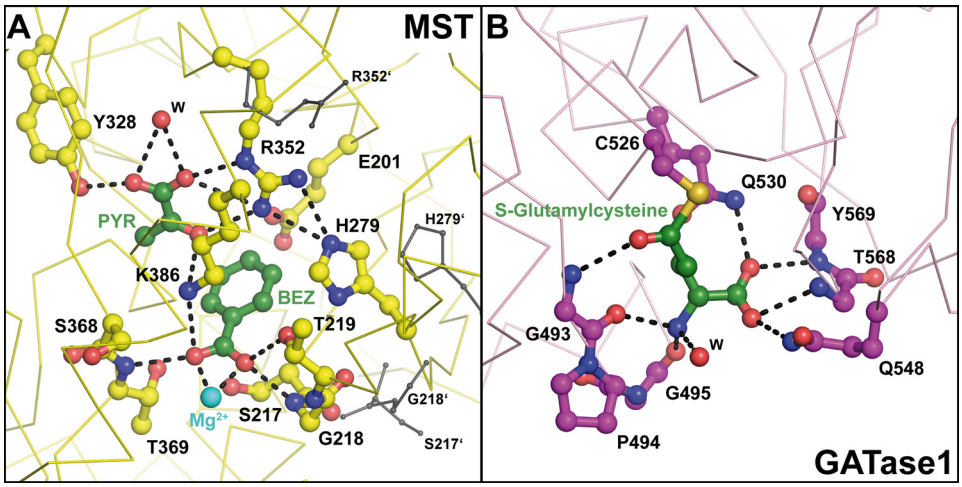

FIGURE 3. **Details of the active sites of PhzE.** *A*, active site of the MST domain. Residues that make hydrogen bonds with pyruvate (*PYR*) or benzoate (*BEZ*) are shown in *ball-and-stick* representation. Mg^{2+} is shown in *cyan*. The positions of important moving residues in the open form are shown in *black*. See Fig. 4*A* for details of the residues coordinating Mg^{2+}. *B*, covalent modification of Cys^{526} in the GATase1 active site.

the unusual arrangement (Fig. 2*C* and supplemental Fig. S3). The intertwined structure is also retained in the closed form, but here the dimer is more outstretched. In fact, this closed conformation fits the SAXS envelope even better than the open form, which is also reflected in a better fit of the calculated scattering curve (χ^2 = 1.5 for the closed conformation *versus* 3.2 for the apo structure; supplemental Fig. S3). This indicates that the quaternary structure observed in the crystal form obtained in the absence of ligands is to a certain extent a crystallization artifact, resulting from the relatively weak interaction between the two MST domains of the dimer. Apparently, this interface can be distorted by crystal packing forces, and the distortion of the open structure manifests itself in a positional change of approximately 60 Å at the outer edge of the GATase1 domain when one of the MST domains from each of the two crystal forms are superimposed (Fig. 2*D*).

Interestingly, in both crystal forms the relative arrangement of the MST and GATase1 domains of the functional unit in PhzE is similar to that found in the heterotetrameric TrpE/G AS, even if the quaternary structures are different. However, because the positions of the two MST domains also differ among the structurally characterized AS (supplemental Fig. S4), this finding alone does not explain the catalytic differences between ADIC synthases and AS.

Chorismate Binding MST Domain—A hallmark of the MST domain is a large β-sandwich structure covered with α-helices from both sides. The active center lies in the core of the domain and is built from residues of both sides of the sandwich together with amino acids from flanking α-helices (Figs. 2*C* and 3A). It was found to contain benzoate and pyruvic acid (Fig. 3*A* and supplemental Fig. S5), even if the closed conformation was obtained by crystallizing PhzE in the presence of chorismic acid. This breakdown of either the substrate chorismic acid or of the product ADIC was also observed in the ligand-bound crystal structure of *Serratia marcescens* AS (PDB ID code 1I7Q) (2). The position and interactions of benzoate and pyruvate are very similar to those of the ADIC isoster isochorismate in the recently published isochorismate synthase EntC structure (28), showing that they serve as a good template for the enzyme/substrate complex (supplemental Fig. S5).

Pyruvic acid is bidentately coordinated to the guanidino group of Arg^{352} and also makes a hydrogen bond with Tyr^{328}. With respect to the unliganded form, the side chain of Arg^{352} adopts a different rotamer conformation to bind pyruvate, whose carbonyl oxygen atom is 3 Å away from C3 of benzoate, clearly indicating that the C-C bond is broken (Fig. 3*A* and supplemental Fig. S5). The carboxylate group of benzoate occupies two positions within the octahedral coordination sphere of an Mg^{2+} cation (Figs. 3*A* and 4*A*). It also involves hydrogen bonds with the amide bonds between Ser^{217} and Gly^{218} and between Ser^{368} and Thr^{369} as well as with the side chains of Ser^{217}, Thr^{219}, and Lys^{386}. Other residues within the first coordination sphere of the ligands include a handful of nonpolar residues together with Glu^{201} and His^{279}. This histidine moves by nearly 4 Å with respect to the unliganded structure to interact with the new rotamer of Arg^{352} (Fig. 3*A*).

GATase1 Domain—The two crystal structures of PhzE allow comparison of the structure of the ligand-free GATase1 domain with that of an intermediate of the catalytic cycle in which Cys^{526} in the active site is covalently modified by a glutamyl moiety (supplemental Fig. S6). Superimposition reveals that only small structural changes accompany ligand binding. With the exception of hydrogen bonds to the side chains of Gln^{530} and Gln^{548}, other polar contacts of the glutamyl group involve backbone atoms of Gly^{493}, Gly^{495}, Thr^{568}, and Tyr^{569} (Fig. 3*B*). The active site itself is located close to the surface and is solvent-accessible in the ligand-free structure. Following a ligand-induced rigid body movement, it becomes secluded through interactions with the MST domain (see below).

Interestingly, in the highest resolution data set of the ligand-bound crystal form collected for this study, we observed additional electron density, including anomalous diffraction in the vicinity of Cys^{526} of the GATase1 active site (see Fig. 6*B* and supplemental Fig. S7*A*). This electron density could be removed by treating the enzyme with EDTA prior to crystallization. Because of the tetrahedral coordination, we assumed that this density results from Zn^{2+} cations, and the presence of zinc was indeed revealed by x-ray fluorescence of crystals (supplemental Fig. S7*C*). Ni^{2+}, which was used to capture His_6-tagged

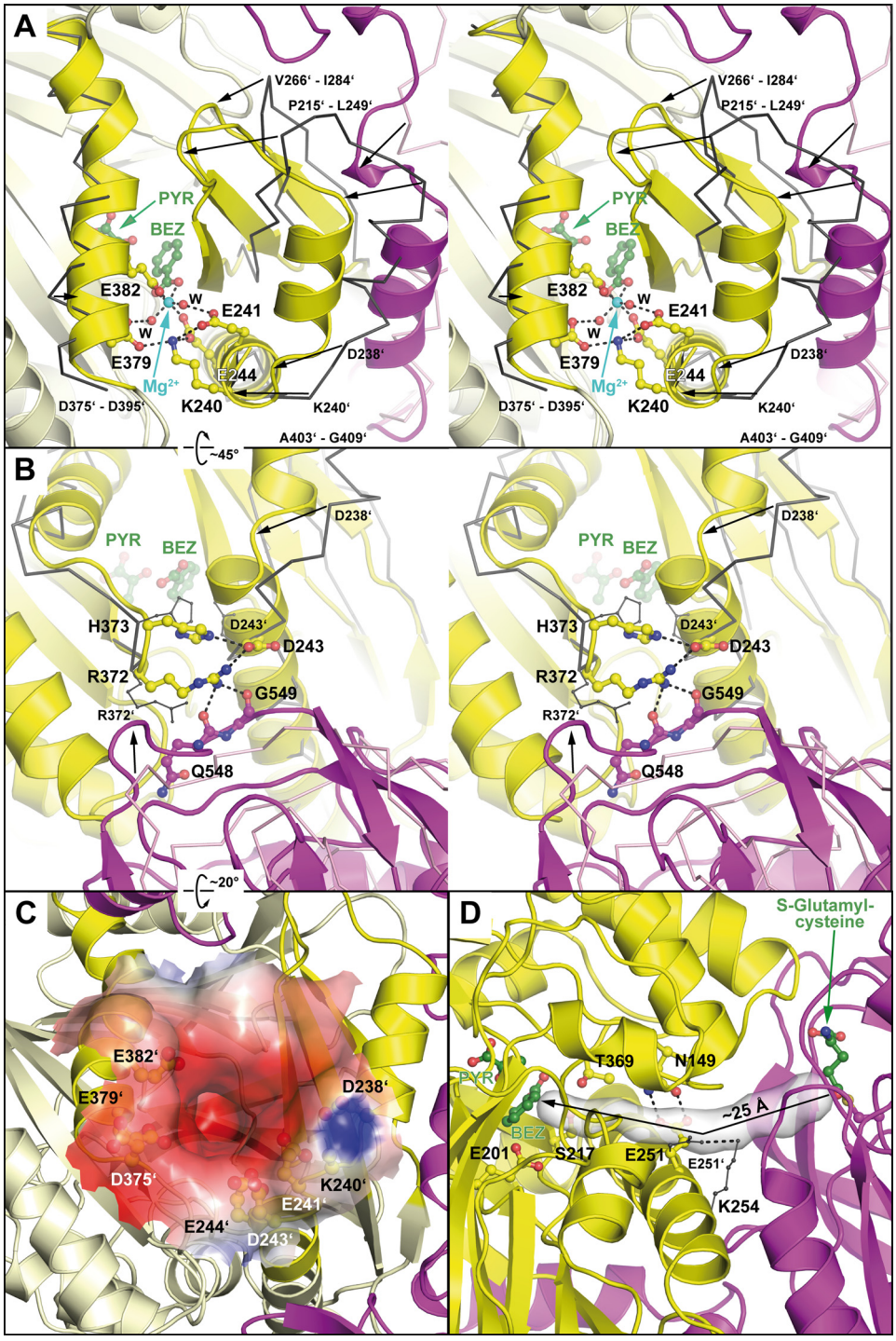

FIGURE 4. **Ligand binding induces structural changes in PhzE.** *A*, stereo plot of the clamp-like closing of the MST active site during ligand binding. Moving parts in the closed form are shown in *yellow*, and their position in the open structure is shown as a *black ribbon*. Residues from the linker of the other monomer are in *magenta*. *Black arrows* indicate the repositioning of single residues. *B*, stereo plot showing the formation of new hydrogen bonds in the MST/GATase1 interface of the ligand-bound structure. Note the reorientation of Asp^{243} with respect to the open form. *C*, cluster of acidic residues and electrostatic surface around the entry to the active site of the MST domain in the open form, calculated with APBS (38). *D*, formation of the ammonia channel between the active centers of MST domain and GATase1 of the second chain. Glu^{251} likely acts as a gatekeeper. The *arrow* indicates the trajectory of NH_3 to Cys^2 of chorismate.

PhzE in the first step of the purification procedure, was not discovered in these experiments (data not shown). It was, however, found that Ni^{2+}, Mn^{2+}, and Zn^{2+} inhibit the enzyme (supplemental Fig. S7*B* and supplemental Table S1). Because the zinc-free and zinc-bound structures of the closed form of PhzE are otherwise identical, the discussion is based on the higher resolution Zn^{2+}-contaminated diffraction data.

Linker—The linker comprises amino acids 396–441 and connects the MST and GATase1 domains at a distance of over 60 Å. It is in part proline- and glycine-rich but also contains α- and η-helical secondary structure. Due to flexibility, it was not possible to trace the linker fully (Gly^{429}–Leu^{439} and Glu^{433}–Leu^{439} missing in chain A and chain B of the apo structure, Gln^{432}–Leu^{439} missing in both chains of the closed structure), but it is clear that

the central α-helix of the linker (residues 403–416) moves in concert with residues Pro^{215}–Leu^{249} when ligands bind the MST domain. Comparison of the open and closed forms reveals that the backbone conformation of amino acids 395–414 differs most strongly between the two structures. These local changes neutralize the large changes in the MST/MST monomer/monomer interface between the two crystal forms of PhzE and keep the relative orientation of the MST and GATase1 domains within the two functional units of the dimer intact (Fig. 2).

DISCUSSION

The data presented here confirm the assignment of PhzE as an ADIC synthase, and the two crystal structures provide insight into structural changes that accompany its catalytic cycle. They also give an opportunity to discuss differences that may lead to the evolution of pyruvate-eliminating and non-eliminating MST enzymes.

First, it is interesting to note that the ligand-bound structure of PhzE fits the SAXS envelope much better than the crystal structure obtained in the absence of substrates, even if the SAXS measurements were performed without ligands (Fig. 2*C* and supplemental Fig. S3). Therefore, the relative arrangement of the two MST/GATase1 functional units found in the apo crystal structure seems to be influenced by crystal packing forces. Only 219 Å^2 of the solvent-accessible surface area are buried in the MST/MST interface of the ligand-bound structure per monomer. Given this very weak interaction, the occurrence of crystal-packing-induced distortions is not very surprising. More contacts between the two MST domains exist in the apo crystal form (471 Å^2 buried per monomer; Fig. 2, *A* and *B*), but these additional interactions involve residues Arg^{221}–Pro^{227}, which undergo ligand-induced movement such that the butterfly shape of the open structure cannot be retained in the crystal structure of the complex (see below).

Structural changes are triggered by the binding of Mg^{2+} and chorismic acid, which apparently bind simultaneously. This is indicated by the observation that no Mg^{2+} was found in the crystal structure of the open form despite being present in the crystallization buffer, and chorismate alone did not show affinity toward PhzE in isothermal titration calorimetry experiments without Mg^{2+} (supplemental Fig. S8). Interestingly, the binding of Mg^{2+}/chorismate is endothermic, *i.e.* entropy-driven. This may be a further indication of structural changes that accompany the process. Obviously, glutamine can only bind second, as shown by the fact that glutamine was not observable in the open form despite being included in the crystallization experiment. Together, this argues for sequentially ordered substrate binding in which Mg^{2+}/chorismate binds first, enabling the GATase1 domain to capture glutamine for hydrolysis.

The octahedral coordination sphere of Mg^{2+} involves a bidentate interaction with the carboxylate group of benzoate, the side chains of Glu^{244} and Glu^{382}, and two water molecules that are held in place by Glu^{241} and Glu^{379} (Fig. 4*A*). These highly conserved acidic residues approach each other with respect to the open structure, leading to a closing of the active center in a clamp-like movement of the α-helix containing Glu^{379} and Glu^{382} on one side and the large structural element from Pro^{215} to Leu^{249} on the other (Fig. 4*A*). It thus is conceivable that neutralization of the negative charges in the formation of the active site in part explains the requirement for Mg^{2+} in the MST enzymes. This is also corroborated by the observation that repositioning of the glutamic acids is accompanied by reorientation of the conserved Lys^{240}, which is disordered and points outward in the apo structure, toward the active center where it interacts with the side chains of Glu^{241}, Glu^{244}, and Glu^{379}, thus adding to the anchoring of both jaws of the clamp (Figs. 3*A* and 4*A*).

Vice versa, the open conformation of PhzE seems to be stabilized by repulsion of negative charges between the helix containing Glu^{379} and Glu^{382} on one side and the highly acidic stretch from Asp^{238} to Glu^{244} on the other (Fig. 4*C*). Of these amino acids, Asp^{238}–Glu^{241} also change their backbone conformation from coil to α-helical structure, which is the most significant local structural rearrangement within the MST domain on ligand binding (Fig. 4*A*). This is likely to add further to the stabilization of the closed form and creates a hinge that triggers the concerted motion of residues Pro^{215}–Leu^{249}. Similar refolding, but to a lesser extent, is also observed in AS (PDB ID codes 1I7Q and 1I7S) (2) and isochorismate synthase (PDB ID codes 3BZM and 3HWO) (28, 29).

Because the structural element Pro^{215}–Leu^{249} contains part of a central strand of one of the β-sheets (Cys^{210}–Tyr^{222}), it pulls the two strands in Val^{266}–Ile^{284} with it, together with residues Ala^{393}–Gly^{419} of the linker, which lines the moving structures in this region. Anchoring of Pro^{215}–Leu^{249} also involves interactions between the carboxylate group of benzoate and the backbone amide between Ser^{217} and Gly^{218}, which leads to a peptide flip with respect to the open conformation (Fig. 3*A*).

The position of Pro^{215}–Leu^{249}/Val^{266}–Ile^{284} of the closed structure is not compatible with the more compressed MST/MST interface observed in the apo crystal structure because it would lead to steric conflicts with Arg^{221}–Pro^{227} of the MST domain in the second chain. Differences in the MST/MST interfaces between the two crystal structures accumulate to a rotation of approximately 50° between the two MST/GATase1 pairs when one MST domain of the open and closed structure are superimposed (Fig. 2*D*). Within the functional units, however, these differences are nearly completely compensated through backbone changes of linker residues Asp^{395}–Arg^{414}.

The MST/GATase1 interface is also subject to changes, yet these are much less pronounced and proceed around a different rotation axis than the crystal-packing-induced MST/MST reorientation. It seems that the refolding within Asp^{238}–Glu^{241} mentioned above also triggers motion of the GATase1 domain because it reorients Asp^{243} outward to form hydrogen bonds with Arg^{372} and His^{373}. As a consequence, the side chain of Arg^{372} repositions to interact tightly with the carbonyl groups of Gln^{548} and Gly^{549} (Fig. 4*B*), which may be sufficient to pull the GATase1 into an 8° rotation with a concomitant 8 Å movement at positions most distant to the rotation axis (Fig. 2*D*).

The clamping motion in the MST fold and the rotation of the GATase1 domain shield both active centers toward the solvent. Because the modification of chorismic acid requires ammonia as a nucleophile, both active centers must coordinate their activities and establish a means for transporting the toxic NH_3 without loss to the environment. Indeed, analysis with CAVER (30) reveals two halves of an ammonia channel that connect the

active centers of the MST and GATase1 domain. The channel is blocked by the side chain of Glu^{251}, which forms two hydrogen bonds with Asn^{149}. Mutation of these residues leads to an inactive enzyme. Glu^{251} adopts a different rotamer in the open structure to interact with Lys^{254}, and the required space for this rotamer is still available in the closed conformation crystallized here (Fig. 4*D*). This implies that Glu^{251} acts as a gatekeeper between the MST and GATase1 active centers, similar to Trp^{74} in glucosamine-6-phosphate synthase from *E. coli* (PDB ID code 1JXA) (31). The closed conformation therefore likely represents a late state of the catalytic cycle in which NH_3 has already been passed to the chorismic acid binding site. The ammonia channel is approximately 25 Å long and ends at C2 of the *si*-face of chorismic acid, thus establishing the stereochemical configuration of ADIC. The nucleophilic attack at C2 is probably assisted by the carbonyl groups of Ile^{216} and Thr^{304} together with the side chains of Ser^{217} and Thr^{369}, which are all positioned to act as hydrogen bond acceptors aiding the deprotonation of NH_3. Protonation of the leaving hydroxyl group at C4 of chorismic acid is achieved by Glu^{201}, whose mutation to glutamine rendered the enzyme inactive (Figs. 3*A* and 5).

It is unclear why benzoate and pyruvate and not chorismate or ADIC were found in the MST active site of the closed crystal form. Although the cleavage of pyruvate seems to be rooted in the tendency of chorismic acid and possibly also of ADIC to undergo sigmatropic reactions including the elimination of pyruvate, the generation of benzoate requires reduction, and the nature of the reducing agent in crystallization of the closed form is unknown at present. However, the breakdown seems associated with an intrinsic enzymatic activity of PhzE because it was not possible to crystallize any of the inactive mutants in the closed conformation. ADIC is a relatively unstable molecule with a half-life of 34 h (22), which is similar to the time required for crystallization. It therefore is likely that the breakdown products originate from ADIC captured in the active center of PhzE before the enzyme has completed its catalytic cycle with product release. This is also corroborated by the observation that Cys^{526} is still covalently modified by glutamine and the fact that it was not possible to crystallize PhzE in the presence of exogenously added benzoate and pyruvate. Further, the breakdown of ADIC seems to be linked to the crystallization conditions because no breakdown products were observed in HPLC analysis of enzyme activity assays.

Further in this context, questions remain concerning the differences between ADIC synthase PhzE and AS, which lyse ADIC to anthranilate and pyruvate (Fig. 1). We tried to employ structural comparisons to identify residues that could convert PhzE into an AS and hence mutated Ser^{217}, Ser^{368}, and Thr^{369} to alanine, alanine, and glycine, respectively, which are the three differences in the first coordination sphere of chorismic acid in which PhzE and AS differ (supplemental Fig. S9). Whereas S368A was unstable, S217A and T369G retained lower levels of ADIC synthase activity and the S368A/T369G double as well as the S217A/S368A/T369G triple mutant were inactive. Increased anthranilate production was not observed, indicating that more subtle differences determine the fate of ADIC in these enzymes. In this respect, it is also interesting to note that the mutation of His^{398} to methionine in AS from *Salmonella enterica* abolishes pyruvate lyase activity nearly completely to create an ADIC synthase (22). However, the corresponding His^{279} is also conserved in PhzE (Fig. 3*A* and supplemental Fig. S9), showing that this residue alone cannot be responsible for the different activities. Convincing theoretical and experimental evidence for a pericyclic pyruvate elimination mechanism in AS and salicylate synthase has been brought forward (32, 33). In this reaction, the enzyme would be expected to act mainly in properly orienting the methylene group of the enolpyruvyl moiety toward the hydrogen atom at C2 of ADIC. In PhzE, binding of the enolpyruvyl group is achieved by the conserved Arg^{352}, which in the closed conformation interacts with His^{279} (Fig. 3*A*). It therefore is conceivable that the H398M mutation in *S. enterica* AS interferes with the proper conformation of ADIC for pyruvate elimination. Because Arg^{352} and His^{279} are conserved in ADIC synthases, however, it seems

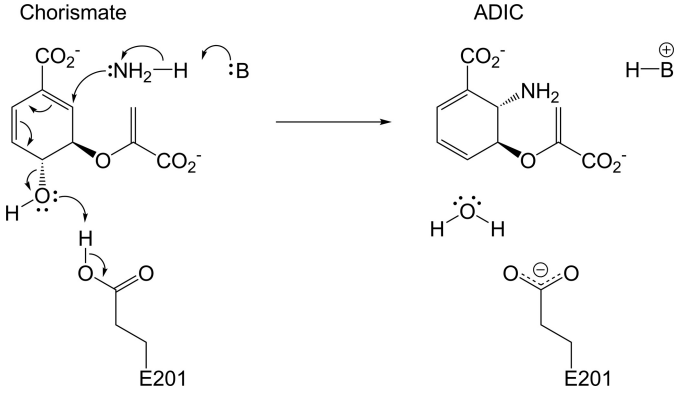

FIGURE 5. **Mechanistic proposal for the generation of ADIC in the active site of the MST domain.** The identity of the base B required for deprotonation of the NH_3 nucleophile is unclear at present.

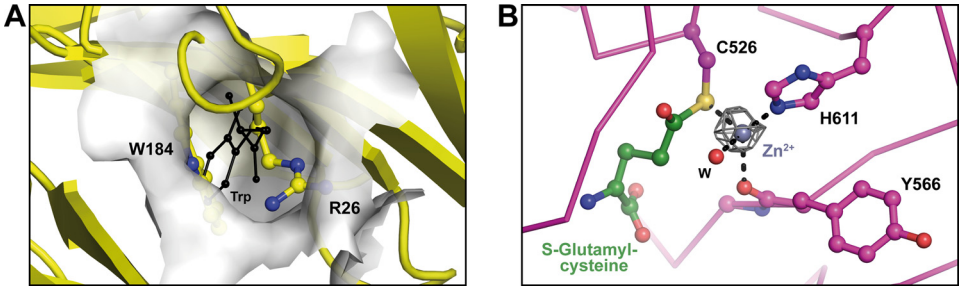

FIGURE 6. **Inhibition of PhzE.** *A*, the allosteric tryptophan binding site of *S. marcescens* anthranilate synthase is blocked by Arg^{26} and Trp^{184} in PhzE. Surface and Trp coordinates (*black*) are from PDB ID code 1I7S (2). *B*, Zn^{2+} (*gray sphere*) binds to the GATase1 active center. Anomalous difference electron density of data collected at 12.4 keV at 5σ are displayed as a *gray mesh*.

likely that the difference between these enzymes lies in the substrate release mechanism, which avoids pyruvate elimination in the ADIC synthases by providing a different release path or by shortening the ADIC residence time in the active center. The latter will be strongly prolonged in protein crystals, explaining why pyruvate elimination was observed in PhzE crystals but not in solution. Although it is tempting to speculate that different release mechanisms are a consequence of different quaternary structures, it has to be mentioned that at least one example of an ADIC synthase in which the MST and GATase1 domains are provided from separate polypeptides is known (27) and that an anthranilate synthase encoded in a single polypeptide with a linker similar to PhzE has been described in the literature (34).

An interesting property of some related AS is their feedback inhibition by L-tryptophan, which is the major downstream product of anthranilate in primary metabolism. We therefore investigated whether PhzE is also feedback inhibited by L-tryptophan or by phenazine-1-carboxylic acid, the end product of enzymes in the *phz* operon. No inhibition was observed with PhzE from *B. lata* or from *Pseudomonas* strains. This presumably is a consequence of a structural variation with respect to AS in that the potential allosteric regulatory site is blocked by the side chains of Arg^{26} and Trp^{184} in PhzE due to differences in the N terminus and an insertion near β-strand 9 (Fig. 6*A* and supplemental Fig. S8). This insertion is also present in the unregulated isochorismate synthases (35).

It is intriguing that we observed Zn^{2+} binding to the GATase1 active center (Fig. 6*B*) and that we could confirm inhibition of PhzE by divalent cations including Zn^{2+}, Mn^{2+}, and Ni^{2+}. The origin of the bound Zn^{2+} is unclear, but it likely stems from the culture media because the only other conceivable source would be $NiSO_4$ used in the first purification step. This chemical contains $<0.002\%$ of contaminating zinc, whereas the accumulated concentration of Zn^{2+} in the cytosol of *E. coli* reaches millimolar values. However, all of this zinc is normally bound (36), showing that PhzE has to compete with other zinc binders to acquire the Zn^{2+} observed here. This could indicate that divalent cations add an unanticipated control layer to the transcriptional regulation by quorum sensing in the overall control of phenazine biosynthesis. Clearly, this aspect will have to be investigated further.

Acknowledgments—We thank Roger S. Goody for continuous support and Petra Geue for excellent technical assistance. We thank the x-ray communities at the Max Planck Institutes of Molecular Phyiology and for Medical Research (Dortmund and Heidelberg, Germany) for help with data collection at the Paul Scherrer Institute (Villigen, Switzerland), which provided generous access to beamline X10SA of the Swiss Light Source. SAXS experiments were performed at beamline X33 of the EMBL outstation at the Deutsches Elektronen-Synchrotron (Hamburg, Germany). E. coli strain KA12 for the overproduction of chorismic acid was a kind gift from Peter Kast. Vinayak Agarwal, Steve M. Fernandes, Frederik Fritsch and Thomas Murray helped in the early stages of the project.

REFERENCES

1. Dosselaere, F., and Vanderleyden, J. (2001) *Crit. Rev. Microbiol.* **27,** 75–131
2. Spraggon, G., Kim, C., Nguyen-Huu, X., Yee, M. C., Yanofsky, C., and Mills, S. E. (2001) *Proc. Natl. Acad. Sci. U.S.A.* **98,** 6021–6026
3. Kerbarh, O., Chirgadze, D. Y., Blundell, T. L., and Abell, C. (2006) *J. Mol. Biol.* **357,** 524–534
4. Raushel, F. M., Thoden, J. B., and Holden, H. M. (2003) *Acc. Chem. Res.* **36,** 539–548
5. Huang, X., Holden, H. M., and Raushel, F. M. (2001) *Annu. Rev. Biochem.* **70,** 149–180
6. Mavrodi, D. V., Blankenfeldt, W., and Thomashow, L. S. (2006) *Annu. Rev. Phytopathol.* **44,** 417–445
7. Mentel, M., Ahuja, E. G., Mavrodi, D. V., Breinbauer, R., Thomashow, L. S., and Blankenfeldt, W. (2009) *Chembiochem* **10,** 2295–2304
8. Doublié, S. (1997) *Methods Enzymol.* **276,** 523–530
9. Kabsch, W. (2010) *Acta Crystallogr. D Biol. Crystallogr.* **66,** 125–132
10. Schneider, T. R., and Sheldrick, G. M. (2002) *Acta Crystallogr. D Biol. Crystallogr.* **58,** 1772–1779
11. de la Fortelle, E., and Bricogne, G. (1997) *Methods Enzymol.* **276,** 472–494
12. Jones, T. A., Zou, J. Y., Cowan, S. W., and Kjeldgaard, M. (1991) *Acta Crystallogr. A* **47,** 110–119
13. Murshudov, G. N., Vagin, A. A., and Dodson, E. J. (1997) *Acta Crystallogr. D Biol. Crystallogr.* **53,** 240–255
14. Emsley, P., Lohkamp, B., Scott, W. G., and Cowtan, K. (2010) *Acta Crystallogr. D Biol. Crystallogr.* **66,** 486–501
15. McCoy, A. J., Grosse-Kunstleve, R. W., Adams, P. D., Winn, M. D., Storoni, L. C., and Read, R. J. (2007) *J. Appl. Crystallogr.* **40,** 658–674
16. Schüttelkopf, A. W., and van Aalten, D. M. F. (2004) *Acta Crystallogr. D Biol. Crystallogr.* **60,** 1355–1363
17. Parsons, J. F., Calabrese, K., Eisenstein, E., and Ladner, J. E. (2003) *Biochemistry* **42,** 5684–5693
18. Roessle, M., Klaering, R., Ristau, U., Robrahn, B., Jahn, D., Gehrmann, T., Konarev, P., Round, A., Fiedler, S., Hermes, C., and Svergun, D. (2007) *J. Appl. Crystallogr.* **40,** S190–194
19. Konarev, P., Volkov, V., Sokolova, A., Koch, M., and Svergun, D. (2003) *J. Appl. Crystallogr.* **36,** 1277–1282
20. Svergun, D. I. (1993) *J. Appl. Crystallogr.* **26,** 258–267
21. Svergun, D. I. (1999) *Biophys. J* **76,** 2879–2886
22. Morollo, A. A., and Bauerle, R. (1993) *Proc. Natl. Acad. Sci. U.S.A.* **90,** 9983–9987
23. Morollo, A. A., Finn, M. G., and Bauerle, R. (1993) *J. Am. Chem. Soc.* **115,** 816–817
24. Roemer, A., and Herbert, R. (1982) *Z. Naturforsch. C Biosci.* **37C,** 1070–1074
25. McDonald, M., Mavrodi, D. V., Thomashow, L. S., and Floss, H. G. (2001) *J. Am. Chem. Soc.* **123,** 9459–9460
26. Pierson, L. S., 3rd, Gaffney, T., Lam, S., and Gong, F. (1995) *FEMS Microbiol. Lett.* **134,** 299–307
27. Van Lanen, S. G., Lin, S., and Shen, B. (2008) *Proc. Natl. Acad. Sci. U.S.A.* **105,** 494–499
28. Sridharan, S., Howard, N., Kerbarh, O., Blaszczyk, M., Abell, C., and Blundell, T. L. (2010) *J. Mol. Biol.* **397,** 290–300
29. Parsons, J. F., Shi, K. M., and Ladner, J. E. (2008) *Acta Crystallogr. D Biol. Crystallogr.* **64,** 607–610
30. Petrek, M., Otyepka, M., Banás, P., Kosinová, P., Koca, J., and Damborský, J. (2006) *BMC Bioinformatics* **7,** 316
31. Teplyakov, A., Obmolova, G., Badet, B., and Badet-Denisot, M. A. (2001) *J. Mol. Biol.* **313,** 1093–1102
32. DeClue, M. S., Baldridge, K. K., Künzler, D. E., Kast, P., and Hilvert, D. (2005) *J. Am. Chem. Soc.* **127,** 15002–15003
33. Zwahlen, J., Kolappan, S., Zhou, R., Kisker, C., and Tonge, P. J. (2007) *Biochemistry* **46,** 954–964
34. Ashenafi, M., Carrington, R., Collins, A. C., and Byrnes, W. M. (2008) *Ethn. Dis.* **18,** S2–9-13
35. Kolappan, S., Zwahlen, J., Zhou, R., Truglio, J. J., Tonge, P. J., and Kisker, C. (2007) *Biochemistry* **46,** 946–953
36. Outten, C. E., and O'Halloran, T. V. (2001) *Science* **292,** 2488–2492
37. Wriggers, W. (2010) *Biophys. Rev.* **2,** 21–27
38. Baker, N. A., Sept, D., Joseph, S., Holst, M. J., and McCammon, J. A. (2001) *Proc. Natl. Acad. Sci. U.S.A.* **98,** 10037–10041

SUPPLEMENTARY MATERIAL

LIGAND BINDING INDUCES AN AMMONIA CHANNEL IN 2-AMINO-2-DESOXYISOCHORISMATE (ADIC) SYNTHASE PHZE

Qi-Ang Li[1], Dmitri V. Mavrodi[2], Linda S. Thomashow[2,3], Manfred Roessle[4], and Wulf Blankenfeldt[1,5]

From the [1]Department of Physical Biochemistry, Max Planck Institute of Molecular Physiology, Otto-Hahn-Straße 11, 44227 Dortmund, Germany, the [2]Department of Plant Pathology, Washington State University, Pullman, WA 99164-6430, U.S.A., the [3]USDA, Agricultural Research Service, Root Disease and Biological Control Unit, Pullman, WA 99164-6430, U.S.A. and the [4]European Molecular Biology Laboratory-Hamburg Outstation, c/o Deutsches Elektronen-Synchrotron, 22603 Hamburg, Germany [5]present address: Lehrstuhl für Biochemie, Universität Bayreuth, Universitätsstraße 30, 95447 Bayreuth, Germany

Overexpression and Purification of *Burkholderia lata* 383 PhzE and *Pseudomonas fluorescens* 2-79 PhzD D38A

phzE was PCR-amplified from genomic DNA of *Burkholderia lata* 383 and cloned into a modified pET plasmid encoding for an N-terminal His_6-tag followed by a Tobacco Etch Virus (TEV) protease site. The protein was overexpressed in *E. coli* Rosetta 2 (DE3) pLysS (MerckBiosciences) for 16 h at 20°C with 0.5 mM isopropyl-β-D-thiogalactopyranoside (IPTG) and then purified by Ni^{2+}-affinity chromatography on HiTrap Chelating resin (GE Healthcare). The His_6-tag was removed with TEV protease and the protein was further purified by size exclusion chromatography on Superdex 200 (GE Healthcare), concentrated to 8.7 mg/ml and stored at -80°C until further usage. Seleno-L-methionine labeled PhzE was obtained by the methionine biosynthesis suppression method (S1). PhzE and PhzD mutants were cloned using pET19m containing native *phz*E or *phz*D as template following the QuickChange protocol (Stratagene). Purification of seleno-L-methionine labeled PhzE and mutants follows the same protocol described above of purifying native PhzE.

Enzymatic Production and HPLC-Purification of 2-Amino-2-desoxyisochorismate ADIC

ADIC was produced enzymatically in 2 mL solution containing 5 mM chorismate, 120 mM glutamine, 10 mM $MgCl_2$ and 50 mM HEPES pH 7.1. The reaction was initiated by adding PhzE to a final concentration of 5 µM. After one hour, the reaction mixture was shock-frozen with liquid nitrogen in 200 µL aliquots and stored at -80 ºC.

To purify ADIC, reverse phase high-performance liquid chromatography (HPLC) experiments

were carried out on a Waters 600 system equipped with a Waters 600S controller, a 717 plus autosampler, a 2487 Dual λ Absorbance Detector and a PRONTOSIL 120-5-C18-AQ 5 µm reverse phase column (Bischoff Analysentechnik). Solvent A was 0.1% TFA in H_2O and solvent B was 0.1 TFA in Acetonirile. The flow rate was set to 1 mL/min and the column was developed with the following gradient: 0 – 2 min: 100% solvent A, 2 – 17 min: 0 – 50% solvent B, 17 – 27 min: 50 – 100% solvent B, 27 – 29 min: 100% solvent B. The integrated software package Empower Pro from Waters was used to process experimental data.

Characterization of ADIC by Electron Spray Ionization Mass Spectrometry (ESI-MS)

ESI-MS measurements were carried out with a LCQ ESI mass spectrometer (Finnigan, SanJose, USA). 0.1% formic acid in water was used as solvent A and 0.1% formic acid in acetonitrile was used as solvent B. Mass spectra were measured in the positive ion detection mode and data were collected at the m/z range between 0 and 600. Data processing and mass calculation was performed using Xcalibur (Thermo Fisher Scientific Inc.) software package.

Crystallization, Data Collection and Structure Determination

Initial crystallization conditions were determined with the JCSG Core I-IV suites (Qiagen). For the ligand free crystal form of PhzE, crystallization conditions were optimized to a reservoir consisting of 0.1 M Bis-Tris propane pH 7.0, 0.2 M potassium thiocyanate and 22% (w/v) PEG 3350, of which 1 µl was mixed with 2 µl of protein solution (8.7 mg/ml) containing 1 mM $MgCl_2$ and 20 mM glutamine and equilibrated against 500 µl reservoir at 20 °C in a hanging drop setup.

Crystals of seleno-L-methionine labeled PhzE were obtained under similar conditions. The ligand-bound crystal form required incubation of protein solution with 50 mM $MgCl_2$, 20 mM chorismate and 25 mM L-glutamine for 30 min on ice and crystallization against a reservoir containing 0.1 M HEPES buffer pH 7.1, 0.2 M $MgCl_2$, and 15% isopropanol at 4 ^oC. Streak seeding was employed to further enhance the quality of these crystals. To remove Zn^{2+} from the GATase1 site, the protein was first incubated with 10 mM EDTA on ice, followed by buffer exchange on an illustra^{TM} NAP-5 column (GE Healthcare). Crystals of ligand-free PhzE were briefly washed in a cryo solution consisting of 0.1 M BTP pH 7.0, 0.2 M potassium thiocyanate, 25% (w/v) PEG 3350 and 5% (w/v) PEG 400 prior to plunging into liquid nitrogen. Cryo solution for Ligand-bound crystals contains 0.1 M HEPES buffer pH 7.1, 0.2 M $MgCl_2$, 15% isopropanol and 20% glycerol.

Crystals of PhzD D38A mutant were obtained from 1µl + 1µl hanging drop equilibrated against a reservoir containing 0.1 M sodium cacodylate buffer pH 6.5, 0.2 M sodium acetate and 25% (w/v) PEG 4000. The crystals were then soaked in a solution containing 0.1 M Bis-Tris pH 6.5, 20% (w/v) PEG 4000, 0.1 M NaCl and 1 mM ADIC for 60 min. Before data collection at 100 K, D38A crystals were briefly washed in a cryoprotecting solution consisting of 0.1 M Bis-Tris buffer pH 6.5, 40% (w/v) PEG 4000 and 0.1 M NaCl.

Diffraction data for PhzE were collected on beamline X10SA of the Swiss Light Source (Paul Scherrer Institute, Villigen, Switzerland) and integrated with the XDS package (S2). The structure of PhzE in the apo-form was determined from MAD data collected at the Se-K-edge, using SHELXD (S3) for locating selenium atoms and SHARP (S4) for initial phasing. The

model was traced in O (S5) and refined with REFMAC5 (S6). Final corrections were applied in COOT (S7). Coordinates for one MST and GATase1 domain, respectively, were used for molecular replacement of the ligand-bound crystal form in PHASER (S8) and MOLREP (S9). For the refinement of this structure in COOT and REFMAC5, restraints dictionaries were generated with PRODRG (S10).

Diffraction data for the D38A mutant of PhzD were collected on an image plate using a rotating copper anode as the x-ray source. The structure was solved by molecular replacement and refined with a similar strategy.

Full data collection and refinement statistics are shown in Tab. 1.

Small Angle X-ray Scattering

SAXS experiments were performed at beamline X33 of the DORIS III storage ring (DESY and EMBL Hamburg, Germany) (S11). The scattering data was recorded by means of an image plate with online readout (MAR345, MarResearch, Norderstedt, Germany). The automated sample handling robot was used for loading protein solution in the X-ray beam (S12). The scattering patterns were measured using a sample - detector distances of 2.4 m, covering the range of momentum transfer $0.1 < s < 4.5$ nm-1 ($s = 4\pi \sin(\theta)/\lambda$, where θ is the scattering angle and $\lambda = 0.15$ nm is the X-ray wavelength). In order to check for inter protein interactions PhzE was measured at 3 and 6 mg/ml concentration. Repetitive measurements of 120sec of the same protein solution were performed in order to check for radiation damage and no aggregation was found during the initial 120sec exposure. This initial exposure frame was taken for further

analysis. The data were normalized to the intensity of the incident beam; the scattering of the buffer was subtracted and the difference curves were scaled for concentration. Corresponding datasets were merged according to the data quality. All the data processing steps were performed using the program package PRIMUS (S13). The forward scattering I(0) and the radius of gyration Rg were evaluated using the Guinier approximation (S14) assuming that at very small angles (s <1.3/Rg) the intensity is represented by I(s) = I(0) exp(-(sRg)2/3). These parameters were also computed from the entire scattering patterns using the indirect transform package GNOM (S15), which also provides the distance distribution function *p(r)* of the particle as defined:

$$p(r)=2\pi\int I(s)sr\sin(sr)ds$$

The molecular mass of PhzE was calculated by comparison with the forward scattering from the reference solution of bovine serum albumin (BSA). From this procedure a relative calibration factor for the molecular mass (MM) can be calculated using the known molecular mass of BSA (66.4 kDa) and the concentration of the reference solution by applying

$$MM_p = I(0)_p / c_p \times \frac{MM_{st}}{I(0)_{st} / c_{st}}$$

where $I(0)_p$, $I(0)_{st}$ are the scattering intensities at zero angle of the studied and the BSA standard protein, respectively, MM_p, MM_{st} are the corresponding molecular masses and c_p, c_{st} are the

concentrations. Errors have been calculated from the upper and the lower I(0) error limit estimated by the Guinier approximation.

Low-resolution models of PhzE were built by the program DAMMIN (S16), which represents the protein as an assembly of dummy atoms inside a search volume defined by a sphere of the diameter D_{max}. Starting from a random model, DAMMIN employs simulated annealing to build a scattering equivalent model fitting the experimental data $I_{exp}(s)$ to minimize discrepancy:

$$\chi^2 = \frac{1}{N-1}\sum_j \left[\frac{I_{\exp}(s_j) - cI_{calc}(s_j)}{\sigma(s_j)}\right]^2$$

where N is the number of experimental points, c a scaling factor and $I_{calc}(s_j)$ and $\sigma(s_j)$ are the calculated intensity and the experimental error at the momentum transfer s_j, respectively. Final a*b initio* shape models for PhzE were obtained applying a two-fold symmetry as constrain to the DAMMIN program. The χ values of the fitting procedure are in the range of 1.50 ± 0.02. Ten independent DAMMIN reconstructions are superimposed using the program package SUBCOMP and DAMAVER (S16) and a most probably PhzE model derived after filtering to the molecular mass of the PhzE dimer.

Isothermal Titration Calorimetry

ITC measurement was employed to determine the dissociation constants of chorismate to PhzE with and without Mg^{2+}. Measurements were performed at 25 °C with a VP-ITC system from MicroCal LLC. For measurement without Mg^{2+}, PhzE was diluted to 100 µM with a buffer containing 50 mM Tris (pH 7.5) and 150 mM NaCl. For measurement with Mg^{2+}, the buffer contained an additional 1 mM $MgCl_2$. Chorismate was dissolved in the same buffer as used for the protein to a final concentration of 1 mM. The system was equilibrated for at least 30 min before the measurement started, and then 2 µl substrate was injected initially, followed by injection of 8 µL at 4 min intervals. Raw data containing enthalpy changes corresponding to the association of chorismate to PhzE were analyzed with Origin version 7 (OriginLab Corporation).

Enzymatic Activity Assays

Activity assays were performed by a modification of the method described before (S17). Reaction mixtures contained 0.1 M HEPES-Na pH 7.0, 1 mM $MgCl_2$, 20 mM glutamine and 1 – 50 µM chorismic acid. The reaction was initiated by addition of ≈100 nM protein and initial velocities were determined by following the increase in absorption at 280 nm. K_M and k_{cat} values were determined by fitting to a Michaelis-Menten equation in GraFit (Erithacus Software). Experiments were repeated at least in triplicate.

Supplementary References

S1. Doublié S (1997) Preparation of selenomethionyl proteins for phase determination. *Meth. Enzymol.* 276:523-530.

S2. Kabsch W (2010) XDS. *Acta Crystallogr. D Biol. Crystallogr.* 66:125-132.

S3. Schneider T, Sheldrick G (2002) Substructure solution with SHELXD. *Acta Crystallogr. D Biol. Crystallogr.* 58:1772-1779.

S4. delaFortelle E, Bricogne G (1997) Maximum-likelihood heavy-atom parameter refinement for multiple isomorphous replacement and multiwavelength anomalous diffraction methods. *Meth. Enzymol.* 276:472-494.

S5. Jones T, Zou J, Cowan S, Kjeldgaard M (1991) Improved Methods for Building Protein Models in Electron-Density Maps and the Location of Errors in These Models. *Acta Crystallogr. A* 47:110-119.

S6. Murshudov G, Vagin A, Dodson E (1997) Refinement of macromolecular structures by the maximum-likelihood method. *Acta Crystallogr. D Biol. Crystallogr.* 53:240-255.

S7. Emsley P, Lohkamp B, Scott WG, Cowtan K (2010) Features and development of Coot. *Acta Crystallogr. D Biol. Crystallogr.* 66:486-501.

S8. McCoy AJ et al. (2007) Phaser crystallographic software. *J. Appl. Crystallogr.* 40:658-674.

S9. Vagin A, Teplyakov A (1997) MOLREP: an Automated Program for Molecular Replacement. *J. Appl. Cryst.* 30:1022-1025.

S10. Schüttelkopf AW, van Aalten DMF (2004) PRODRG: a tool for high-throughput crystallography of protein-ligand complexes. *Acta Crystallogr. D Biol. Crystallogr.* 60:1355-1363.

S11. Roessle M et al. (2007) Upgrade of the small-angle X-ray scattering beamline X33 at the European Molecular Biology Laboratory, Hamburg. *J. Appl. Crystallogr.* 40:s190-s194.

S12. Round AR et al. (2008) Automated sample-changing robot for solution scattering experiments at the EMBL Hamburg SAXS station X33. *J. Appl. Crystallogr.* 41:913-917.

S13.Konarev P, Volkov V, Sokolova A, Koch M, Svergun D (2003) PRIMUS: a Windows PC-based system for small-angle scattering data analysis. *J. Appl. Crystallogr.* 36:1277-1282.

S14.Guiner A, Fournet G (1955) *Small angle scattering of X-ray* (Wiley, New York).

S15.Svergun DI (1993) A direct indirect method of small-angle scattering data treatment. *J. Appl. Crystallogr.* 26:258-267.

S16.Svergun DI (1999) Restoring low resolution structure of biological macromolecules from solution scattering using simulated annealing. *Biophys. J.* 76:2879-2886.

S17.Morollo A, Bauerle R (1993) Characterization of Composite Aminodeoxyisochorismate Synthase and Aminodeoxyisochorismate Lyase Activities of Anthranilate Synthase. *Proc. Natl. Acad. Sci. U.S.A.* 90:9983-9987.

Supplementary Figures and Tables

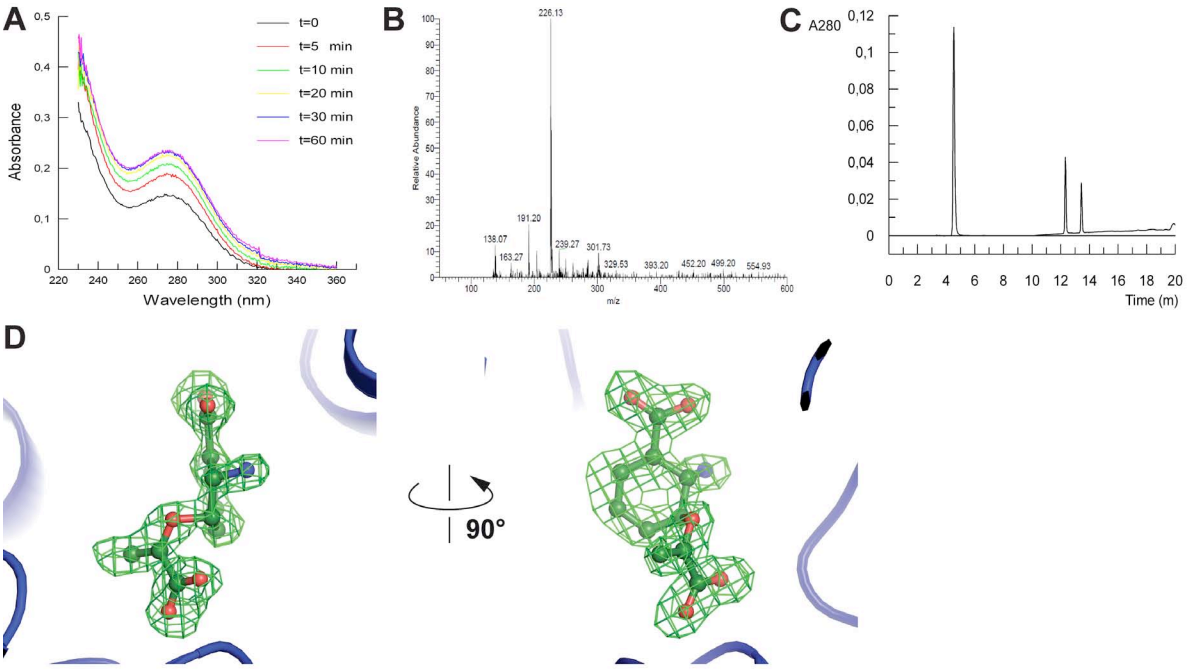

Fig. S1 Characterization of ADIC. (A) UV spectra of PhzE catalyzed reaction. Buildup of ADIC was monitored by increasing of absorption at 280 nm. (B) ESI-MS spectrum of purified ADIC. (C) HPLC chromatogram of PhzE/D reaction. PhzD was added to PhzE reaction solution 10 min after reaction started. Conversion of ADIC to DHHA was observed. (D) $|F_OF_C|$ difference electron density at 2 σ before incorporating ADIC into the model.

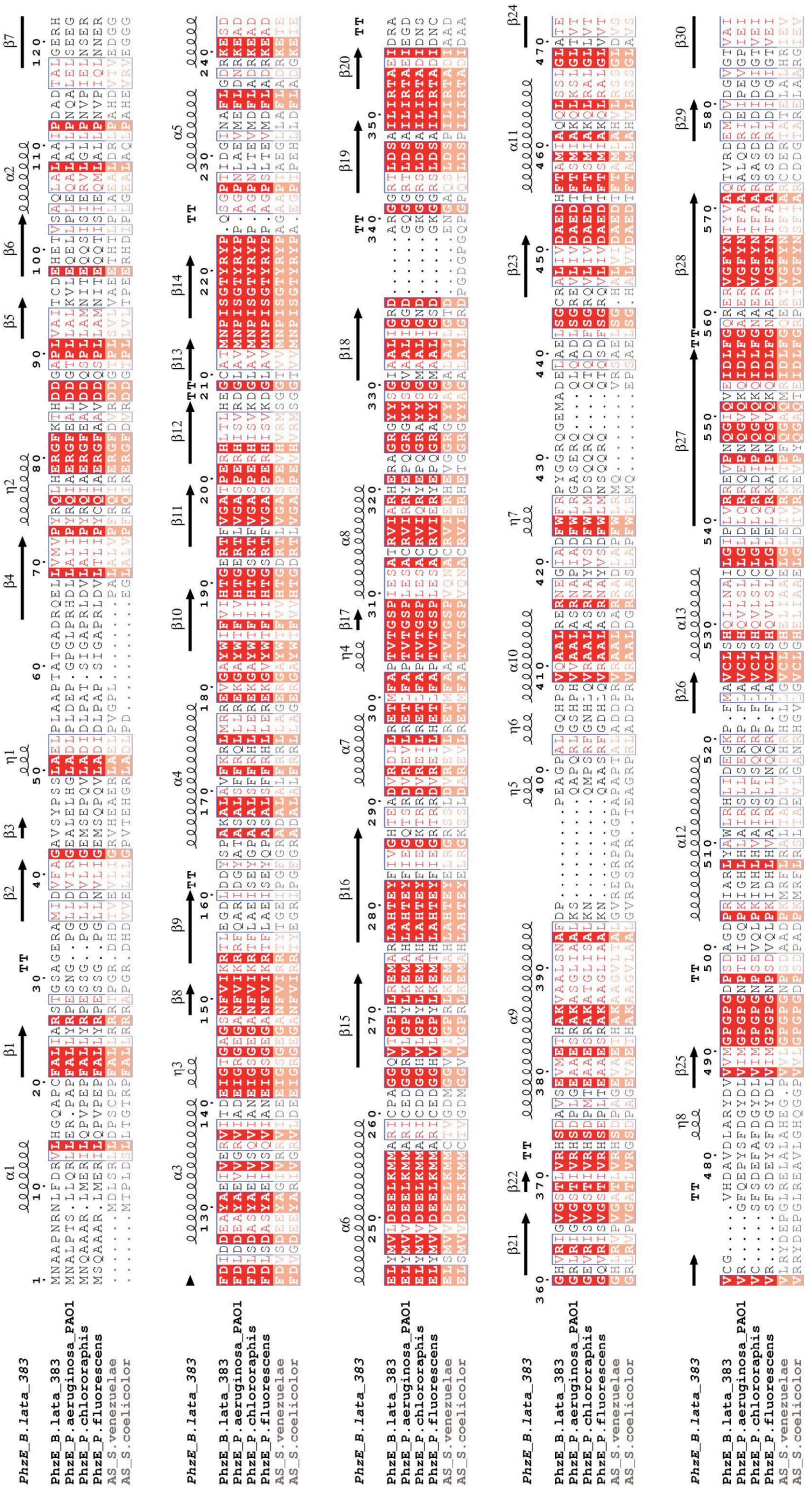

Fig. S2 Sequence alignment of PhzE proteins (black) and two of the related MST/GATase1-fused anthranilate synthases (gray). Secondary structure elements of PhzE *B. lata 383* are shown on top.

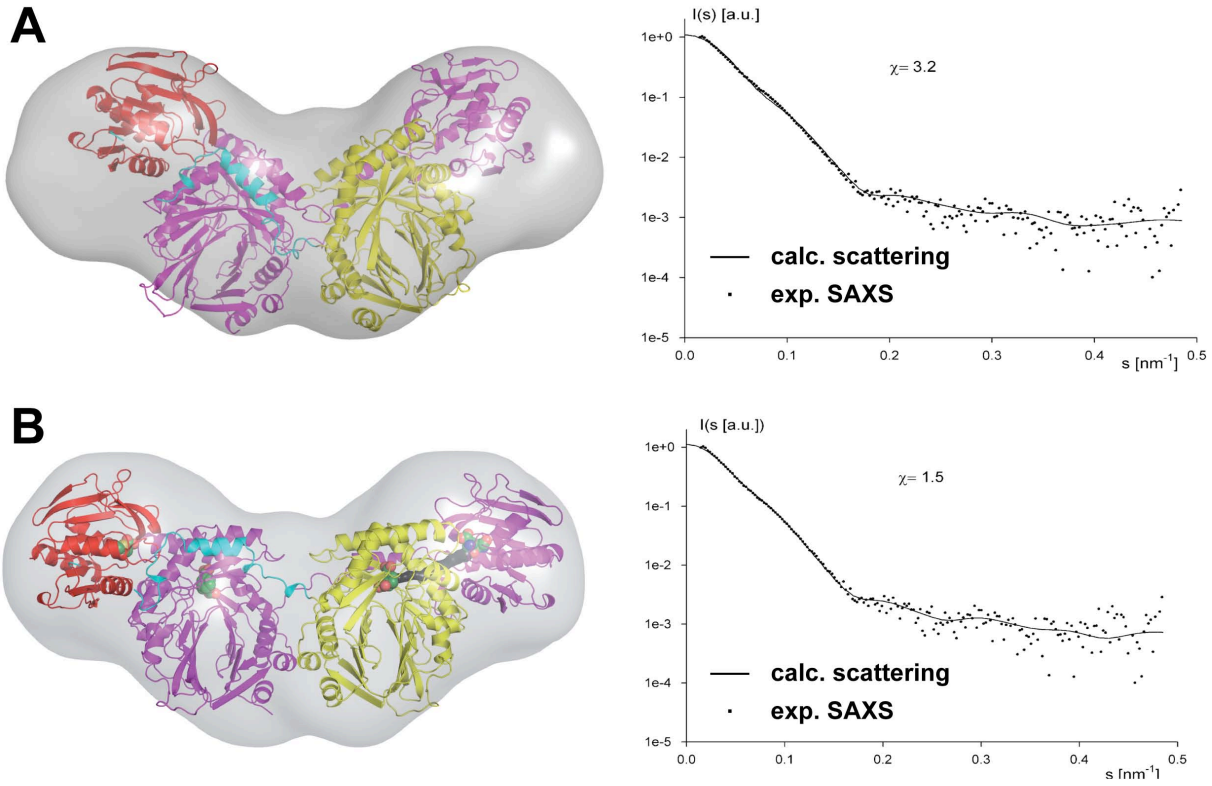

Fig. S3 Small-angle x-ray scattering of PhzE. The SAXS envelope is shown in grey. (A) Fit of the apo crystal structure. (B) Fit of the ligand-bound crystal structure. The graphs show experimental and calculated scattering curves. Note that the ligand-bound crystal structure fits the SAXS data better, even if the scattering was recorded in the absence of ligands.

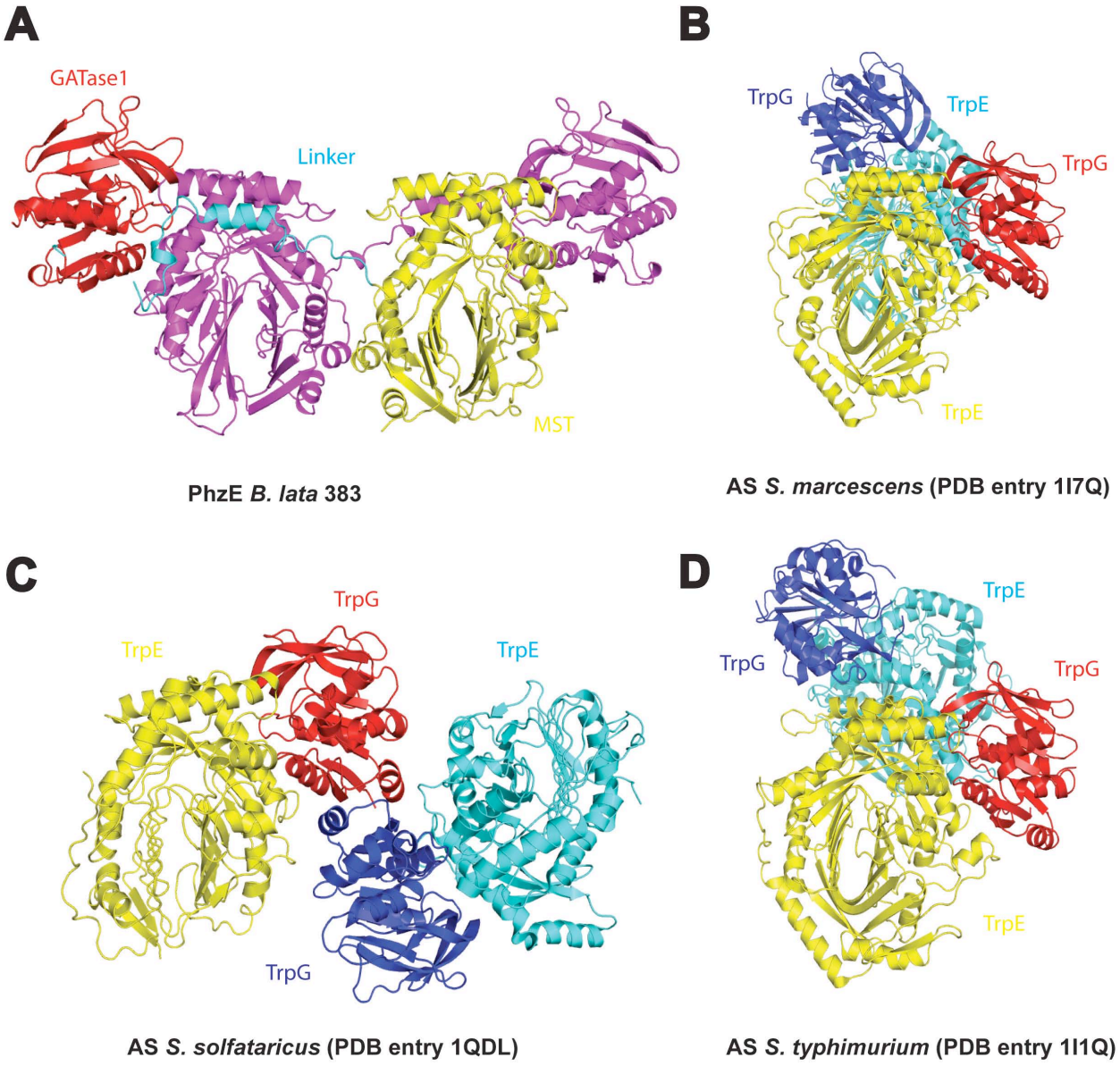

Fig. S4 Quaternary structure comparison of PhzE with heterotetrameric TrpE/G anthranilate synthases (AS). (A) PhzE from *Burkholderia lata* 383. (B) AS from *Serratia marcescens*. (C) AS from *Sulfolobus solfataricus*. (D) AS from *Salmonella typhimurium*. All structures were superimposed on the "yellow" MST domain of PhzE. Note that while the quaternary structures are different the relative arrangement within the MST/GATase1 functional units is identical.

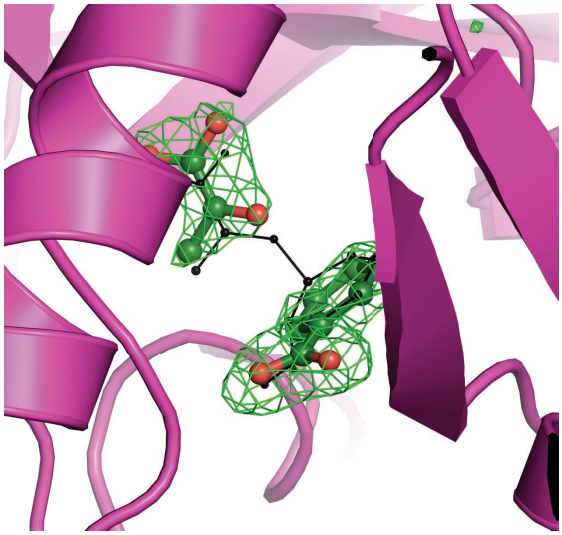

Fig. S5 Superposition of benzoate and pyruvate to isochorismate (black) at the active center of MST domain. $|F_OF_C|$ difference electron density of benzoate and pyruvate is displayed at 3.5 σ. Isochorismate-coordinates are from PDB entry 3WHO.

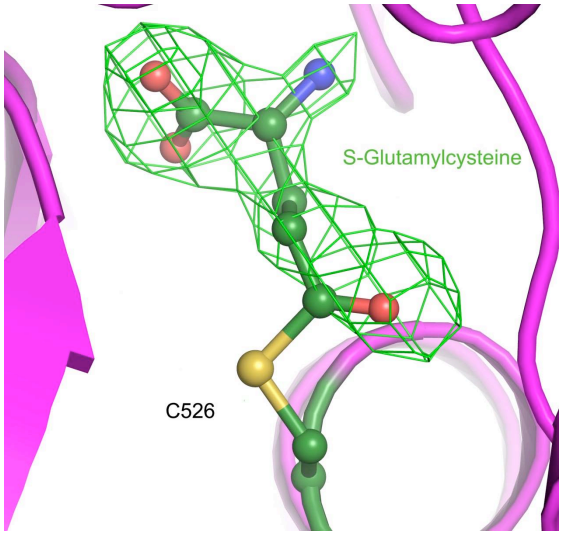

Fig. S6 $|F_OF_C|$ difference electron density of covalently bound glutamyl moiety at 2 σ.

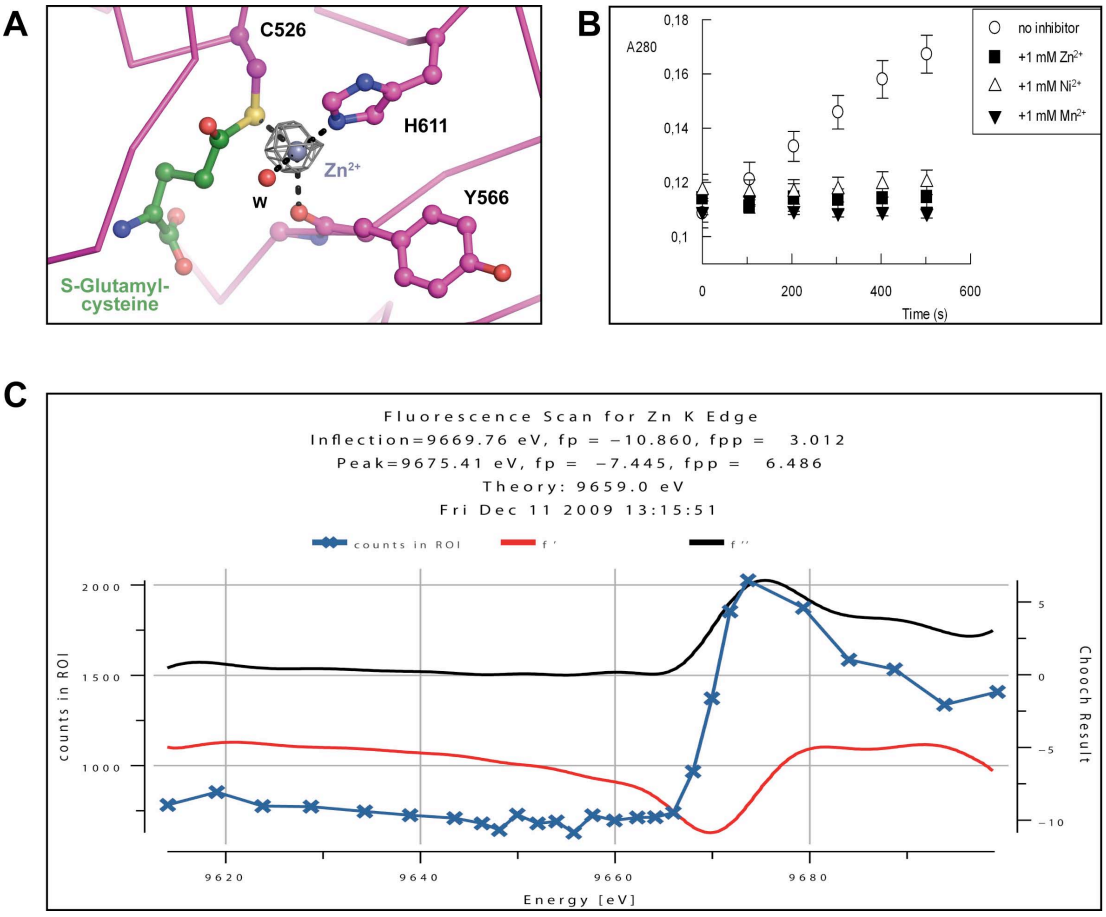

Fig. S7 Divalent cations inhibit PhzE. (A) Zn^{2+} (grey sphere) binds to the GATase1 active center. Anomalous difference electron density of data collected at 12.4 keV at 5σ is displayed as a grey mesh. (B) Inhibition of PhzE by divalent cations. All reaction solutions contain 0.1 M HEPES pH 7.0, 10 mM *L*-glutamine, 50 µM chorismate and 1 mM Mg^{2+}. (C) X-ray fluorescence spectrum a PhzE crystal in the closed conformation at the zinc K-edge. The protein has not been treated with EDTA prior to crystallization.

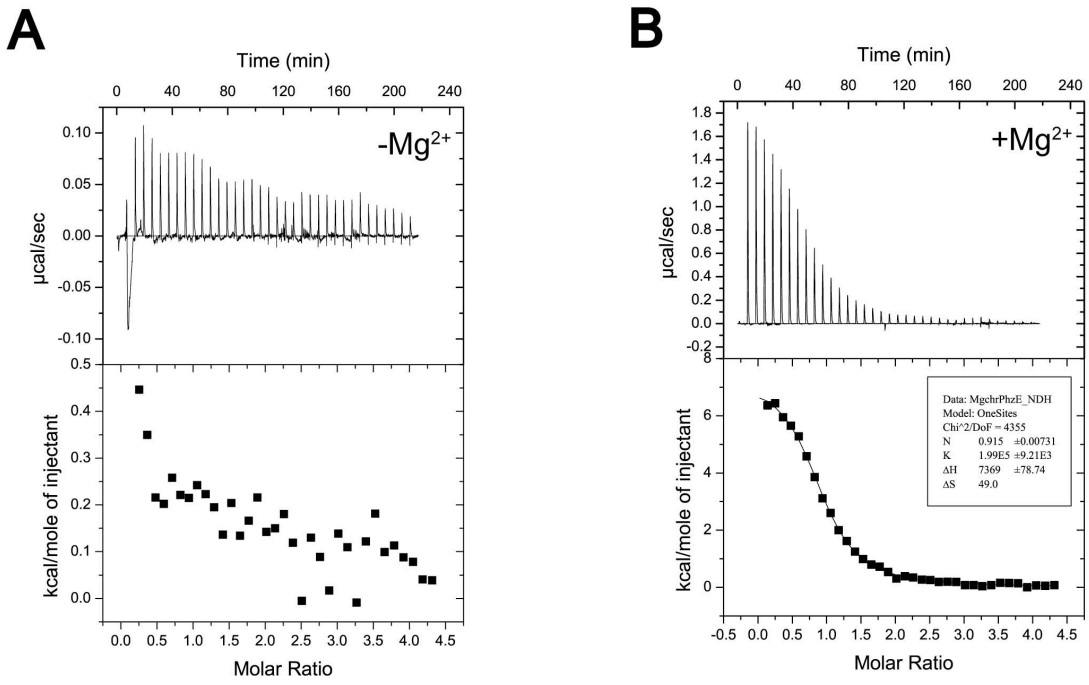

Fig. S8 ITC titration experiment of chorismate without Mg^{2+} (a) and with Mg^{2+} (b).

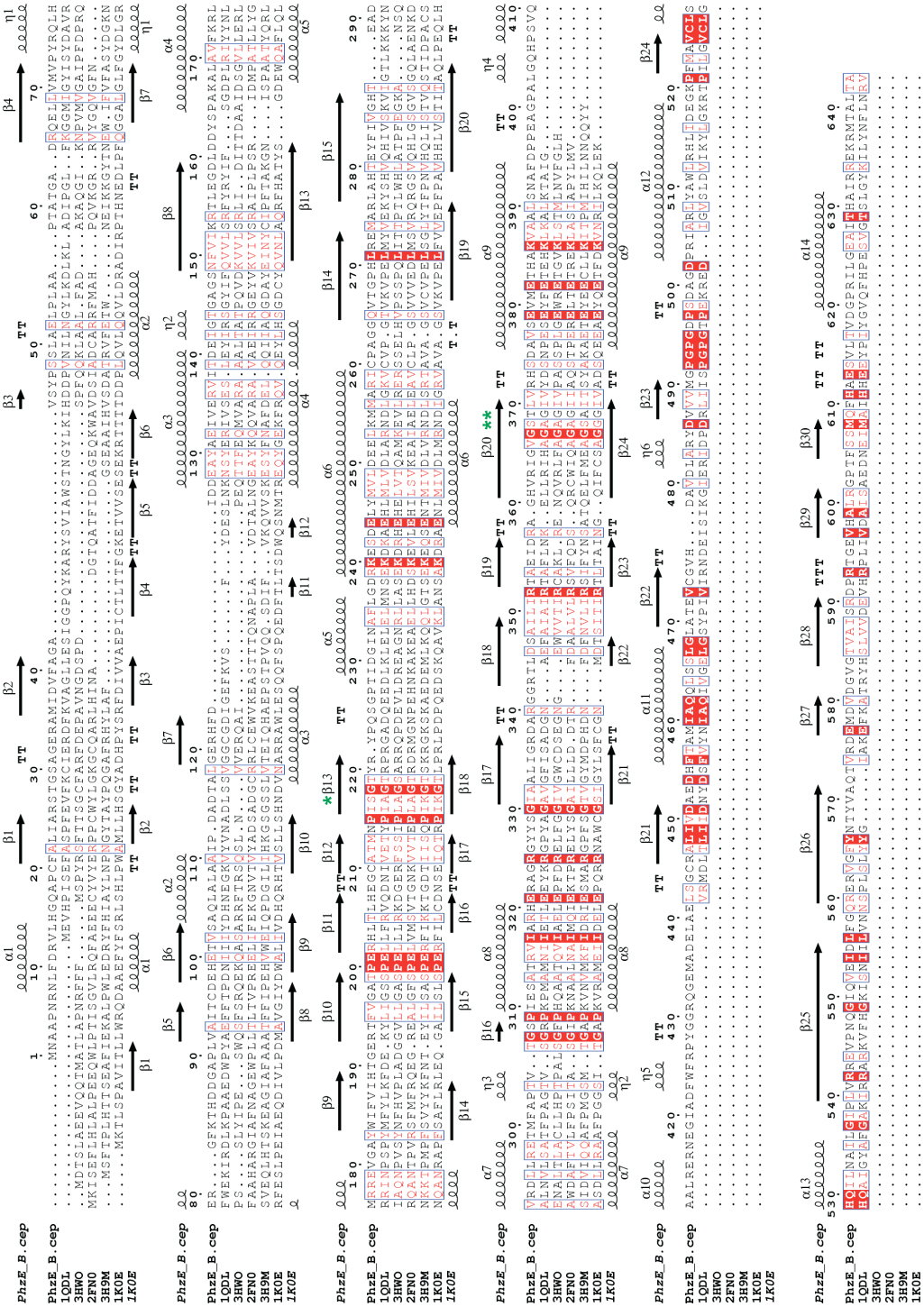

Fig. S9 Structure-based sequence alignment of various MST enzymes. Green stars (*) indicate amino acids in the first coordination sphere of the chorismate binding sites in which ADIC-synthase PhzE differs from anthranilate synthases. PDB entry 1QDL is an anthranilate synthase, 3HWO a isochorismate synthase, 2FN0 a salicylate synthase,

3H9M a p-aminobenzoate synthase and 1K0E a 4-amino-4-deoxychorismate synthase.

Enzyme	K_m **(µM)**	k_{cat} **(s^{-1})**	k_{cat}/K_m **($M^{-1}s^{-1}$)**	**Description**
PhzE	2.4 ± 0.51	0.25 ± 0.013	1.0×10^5	Metal-free
PhzE (untreated)	3.0 ± 0.48	0.13 ± 0.006	4.3×10^4	Zn^{2+} -bound
E201Q	n.d.	n.d.	n.d.	Catalytic residue
S217A	4.0 ± 1.02	0.11 ± 0.008	2.8×10^4	mutation according to AS
E241A	2.3 ± 0.47	0.034 ± 0.002	1.5×10^4	Involved in Mg^{2+} coordination
E244A	n.d.	n.d.	n.d.	Involved in Mg^{2+} coordination
E251Q	n.d.	n.d.	n.d.	Gate-keeping residue of the ammonia channel
E251A	n.d.	n.d.	n.d.	
S368AT369G	n.d.	n.d.	n.d.	Double-mutation according to AS
S217AS368AT369G	n.d.	n.d.	n.d.	Triple-mutation according to AS
T369G	3.5 ± 1.86	0.013 ± 0.002	3.7×10^3	mutation according to AS
E379A	n.d.	n.d.	n.d.	Involved in Mg^{2+} coordination
E382A	1.7 ± 0.57	0.022 ± 0.002	1.3×10^4	Involved in Mg^{2+} coordination
TrpE/G	4.0	9.3	2.3×10^6	AS from *S.typhimurium*
Irp9	4.2	0.13	3.2×10^4	SS from *Y.enterocolitica*
EntC	7 ± 0.8	0.62	8.8×10^4	IS from *E.coli* involved in enterobactin biosynthesis
MenF	192 ± 7	3.6 ± 0.08	1.9×10^4	IS from *E.coli* involved in menaquinone biosynthesis

Tab. S1 Kinetic parameters of PhzE, PhzE mutants and related enzymes with respect to chorismate. Values for related enzymes (TrpE/G, Irp9, EntC & MenF) have been taken from the literature.

	Se-MAD[1]		
Data collection	Se-peak	Se-inflection	Se-remote
Space group		$P6_222$	
Cell dimensions			
a, *b*, *c* (Å)		171.5, 171.5, 217.2	
α, β, γ (°)		90, 90, 120	
Wavelength	0.97895	0.97957	0.97793
f'	-7.51	-13.20	-2.58
f''	10.75	5.12	4.97
Resolution (Å)	20 – 3.6	20 – 4.0	20 – 4.0
(highest shell)	(3.7 – 3.6)	(4.1 – 4.0)	(4.1 – 4.0)
R_{svm} (I)	17.4 (93.7)	14.4 (55.7)	18.5 (83.2)
R_{merge} (F)	12.8 (52.7)	13.3 (41.7)	18.2 (62.1)
I / σ(I)	15.2 (3.5)	13.6 (4.1)	11.2 (2.8)
Completeness (%)	99.9 (99.9)	99.9 (100)	99.9 (100)
Redundancy	13.6 (13.6)	7.3 (7.3)	7.3 (7.3)

[1]Data collections statistics for MAD data refer to unmerged Friedel.

Tab. S2 Statistics of PhzE Se-MAD data collection.